Paper No.
08323

NACE INTERNATIONAL CORROSION 2008 CONFERENCE & EXPO

Cathodic Behavior of Stainless Steel 316LN Reinforcing Bars In Simulated Concrete Pore Solutions

Fushuang Cui
E.I. DuPont
Experimental Station 302/117D
Rt 141 and Henry Clay
Wilmington, DE 19803

Alberto A. Sagüés
Department of Civil and Environmental Engineering
University of South Florida
4202 E. Fowler Ave. ENB 118
Tampa, FL 33620

ABSTRACT

The high corrosion resistance of stainless steel (SS) reinforcing bars is widely recognized. However, little information is available on how much cathodic current a passive SS rebar assembly could produce to support a local anode as corrosion eventually starts. The ability of SS to perform as a cathode would have a direct impact on the corrosion rate of the anodic region. To address this issue, the cathodic behavior of type 316LN SS reinforcing bars in simulated concrete pore solutions was explored using the cyclic potentiodynamic polarization technique. The cathodic efficiency of sandblasted or as-received SS rebar was found to be much smaller than that of as-received carbon steel (CS) rebar. However, high temperature oxide scales, especially those formed at 700 ^{o}C, significantly increased the cathodic efficiency of SS. The effect of temperature and pH on cathodic efficiency of sandblasted SS rebar was secondary compared to that of the presence of oxide scales formed at high temperatures. The oxygen reduction rate on sandblasted SS increased upon addition of chloride ions in solution

Keywords: Corrosion, cathodic behavior, stainless steel, carbon steel, galvanic corrosion, polarization, reinforcing bar

INTRODUCTION

Numerous investigations have reported that solid austenitic stainless steel (SS) rebar, comparing to traditional carbon steel (CS) rebar, has superior corrosion resistance in chloride contaminated concrete. [1-3] When passive, both SS and CS have comparable corrosion potentials and the coupling of the two materials is of little effect on the corrosion behavior of either material. However, when used together in a structure subject to chloride ingress from deicing salts or seawater, CS could start to corrode while SS still remains passive, as the former has much lower corrosion resistance. In such a scenario, if CS and SS are electrically connected, a galvanic corrosion cell will form with the SS as the cathode, and corrosion of the CS could be significantly accelerated. The extent of this acceleration, however, depends highly on the cathodic behavior of the SS.

Figure 1 illustrates two alternative idealized galvanic coupling scenarios. Lines A, C1 and C2 respectively denote the polarization curves of one (purely) anodic corroding spot on a rebar and two alternative (purely) cathodic conditions for the passive remainder of the rebar assembly,. For simplicity, all reactions are assumed to be activation limited, operating far away from their respective equilibrium potentials, with little resistive polarization, and with the same Tafel slope for C1 and C2. I_1 and I_2 then correspond to the corrosion currents of the anode when it is in contact with cathode C1 and C2, respectively. Clearly, coupling with the stronger cathode C2 Increases the corrosion current (and corresponding current density and corrosion rate) of anode A respective to coupling with C1. The acceleration depends on the relative polarizability of the anodic and cathodic regions, but it is always stronger the further the polarization curve of C2 is displaced to the right compared with that of C1. The relative ability of a cathode to accelerate corrosion of an anode, measured by the amount of cathodic current density provided at a given polarization level will be called the cathodic efficiency in the context of this paper[1]. Thus as shown, C2 has higher cathodic efficiency than C1.

Bertolini et al [4-6] and Pedeferri et al [7-8] investigated cathodic behavior of type 304 and 316 SS in both simulated concrete pore solutions and concrete, and concluded that the cathodic efficiency of passive bars of both SS types was significantly lower than that of passive CS bars. Jaggi et al [9] investigated cathodic behavior of type 304 SS disks (grounded surface) in simulated concrete pore solution and drew a similar conclusion. Recent work by Sagüés[19] with finely polished carbon steel and Cr alloys saw similar findings too. Therefore, the galvanic coupling between passive SS and active CS would appear to be less troublesome than the coupling between passive CS and active CS in ordinary reinforcing applications. However, the cathodic efficiency of SS was found to depend strongly on its surface condition. For example, Bertolini and Pedeferri reported that the cathodic efficiency of heat treated (air exposure to 700^{o}C for 10 minutes, simulating a welding treatment) type 316L SS was high, comparable to that of CS. However, these investigations often used polished small disks (solution tests) or smooth round bars (concrete tests) which may have a significantly different starting surface makeup from mill-rolled rebar.

To explore the effect of actual manufactured conditions, this investigation determined the cathodic behavior of corrugated, commercially produced SS rebar in its as-received surface condition and with various subsequent treatments. The material was Type 316LN SS rebar,

[1] The term "efficiency" as used here does not refer to which fraction of the cathodic current contributes to the formation of a given reaction product, as the term may be employed in some branches of electrochemistry.

and the cathodic behavior was evaluated in simulated concrete pore solutions using principally the cyclic potentiodynamic polarization technique (CPP). The impact of solution pH, temperature, chloride concentration and exposure time was also explored. CS specimens were tested for comparison.

EXPERIMENTAL

Materials and Preparation

Type 316LN SS and ASTM A615 CS bars were investigated. All the bars were corrugated and had a nominal diameter of 19mm (No.6 bars). The as-received SS bars were acid pickled by the manufacturer, and the CS bars had intact mill scale (CS rebar in this condition is commonly called "black bar"). Table 1 lists the bulk chemical compositions. The bars were cut into 15cm long specimens, and electric contact to each specimen was made through a copper wire attached to one cut end that was then embedded in metallographic epoxy compound caps. The other cut end was left open (120 grit SiC paper ground finish). Figure 2 illustrates the configuration of the specimens. The following surface conditions were tested:

For SS specimens,

- As-received
- Sandblasted
- Heated in air at 700^{o}C for 10 minutes (simulating welding effects)
- Heated in air at 1000^{o}C for 10 minutes (simulating a generic hot rolling situation)

For CS specimens,

- As-received
- Sandblasted

Model Solutions

Specimens with each surface condition listed above were tested in Type 1 simulate concrete pore solution (SPS1, pH~12.6) at room temperature (22±2^{o}C). Additional tests of sandblasted SS specimens were performed in SPS1 at 40±2^{o}C and type 2 simulated concrete pore solution (SPS2, pH~13.5) at 22±2^{o}C to assess the effect of temperature and pH. Selected portions of base solution SPS1 had NaCl added to obtain chloride concentrations of 1, 3, 5 and 8 wt.% All the solutions were initially naturally aerated but minimizing subsequent surface area in contact with external air, and with enough alkaline reserve, to avoid significant changes from interaction with atmospheric CO_2. The chemical composition of the base SPS1 and SPS2 model solutions is given in Table 2.

Testing

Test cells had typically 90 cm^3 of electrolyte. In order to minimize complicating factors inherent in conventional potentiodynamic polarization technique, the CPP technique was employed to characterize cathodic behavior. In a typical test the potentiostat-controlled potential of a specimen was scanned from E_{oc} (open circuit potential) to E_{oc}-0.3 V and then

back to E_{oc}. The purpose of the tests was to obtain a cathodic polarization curve representative of behavior at the metal-electrolyte interface under steady state conditions. Because the tests were performed in a finite space and finite time interval, complicating factors arise that change the shape of the CPP with respect to those corresponding to the intended conditions. Two notable factors were considered:

1. The resistance of the testing medium between the testing specimen and the reference electrode (R_s). When a current I is impressed during a CPP test, the actual potential E' applied to the interface differs from the programmed value E by IxR_s ($E'=E-IxR_s$). However, the values of R_s in the test cells used were small (typically < 10 ohm) and total currents rarely exceeded 300 μA so this "IR drop" effect was usually < 1mV and therefore was neglected.

2. The effective interfacial capacitance of the metal-electrolyte interface. Upon a potential step change some of the interface current demand vanishes with time. That part of the current demand, not related to the main steady state cathodic reaction, is due to the double layer capacitance plus other possible processes such as buildup or dissolution of oxide films toward establishment of a new steady state. On first approximation, the effect may be considered as introducing an extra non-Faradaic current I_{nF} (I_{nF} =-C x dE/dt) into the measured current where C is an effective interfacial capacitance. Due to the presence of I_{nF}, as shown in Figure 3, the forward scan E-i curve does not completely overlap with the backward scan E-i curve. However, since the scan rate dE/dt is equal but of opposite signs in the forward and reverse scans, at a given potential the value of I_{nf} incurred during the forward scan is the opposite of I_{nf} in the backward scan. Therefore, this complicating factor can be largely removed for purposes of displaying polarization curves by calculating the average values (defined as $i_{average}$) of $i_{forward}$ (the current density during the forward potential scan) and $i_{backward}$ (the current density during the backward potential scan) at the same potentials. Thus all CCP curves presented hereafter are E-$i_{average}$ curves. Apparent Tafel slopes were estimated from the lower sections of such curves (between E_{oc}-0.15V and E_{oc}-0.25V).

In order to select a proper scan rate, trial CPP tests using three different scan rates (0.05 mV/s, 0.167 mV/s and 0.5 mV/s) were performed on sandblasted SS specimens. As shown in Figure 4, the variation in scan rate appeared to have little impact on the shape of the E-$i_{average}$ CPP curves. Thus a scan rate of 0.167 mV/s (a value same as in ASTM G 5 for potentiodynamic anodic polarization measurement) was conveniently selected as the normal testing scan rate.

Electrochemical Impedance Spectroscopy (EIS) was performed at the E_{oc} on selected specimens just before the CPP test to obtain further insight on the rebar corrosion condition. The EIS frequency range was from 300 kHz to as low as 0.3 mHz. The simple equivalent circuit shown in Figure 5 was used to fit the EIS spectra in order to estimate values of R_s (the solution resistance between reference electrode and a specimen), R_p (polarization resistance of a specimen, Y_o and n (two components of the constant phase element). Values of R_s were used to estimate IR drops incurred during polarization as indicated above with the conclusion that the IR drops were very small so correction was not performed. Values of R_p were used to calculate an apparent corrosion rate

$$i_{corr} = B/(R_p x S) \qquad (1)$$

where B is the Stern-Geary [10] constant and was chosen to be 52 mV, a value often used for passive steel in concrete.[11-12] S is the geometric surface area of a specimen.

Both CPP and EIS tests used a saturated Calomel electrode (SCE) as reference electrode and a high-density graphite rod as counter electrode. At least duplicate specimens were used, and the reproducibility was generally good so trends shown in this paper are representative of all replicates unless exceptions are indicated. Unless stated otherwise, all the specimens were conditioned in the corresponding model solution for two days before the electrochemical test(s) was performed.

RESULTS

Figure 6 shows a typical CPP curve of sandblasted SS rebar compared with a typical CPP curve of as-received CS rebar. Twelve sandblasted SS specimens and three as-received CS specimens were tested. For SS specimens, the CPP curves were always similar in shape, corresponding essentially to simple activation polarization with an apparent Tafel slope ~130 mV/dec. The lack of significant concentration polarization reflects the relatively mild polarization regime examined, which resulted in moderate maximum current density values. This apparent Tafel slope of sandblasted SS is comparable to that observed by Pedeferri et al [8] from Potentiostatic Polarization (PSP) but smaller than the one (~230 mV/dec) reported by Jaggi et al [9] who used potentiodynamic polarization (PDP) with a 1 mV/s scan rate. For CS specimens, the CPP curves of the three CS specimens were very similar in shape and a Tafel slope ~190mV/dec was estimated.

Clearly, at the same potentials the cathodic current densities supported by sandblasted SS specimens were typically much smaller that those supported by as-received CS specimens. For example, at –400 mV (vs. SCE), the average cathodic current density of the 12 SS specimens was 0.29 $\mu A/cm^2$ and that of the three CS specimens was 1.52 $\mu A/cm^2$. Per the concepts illustrated in Figure 1, the CPP results indicate that sandblasted SS is markedly less capable than as-received CS of supporting corrosion at an anode.

Figure 7 shows typical CPP curves of SS specimens with various surface conditions compared with a typical CCP curve of an as-received CS specimen. While the Tafel slopes are not very different from each other, the cathodic efficiency of SS appears to depend highly on surface condition. At -400 mV, for example, the average cathodic current densities of SS with as-received surface (three specimens tested), with oxide scales formed at 700 ^oC (two specimens tested), and with oxide scales formed at 1000^oC (two specimens tested) were 0.40, 2.59, 0.38 $\mu A/cm^2$, respectively. In contrast, the average cathodic current density of sandblasted SS was 0.29 $\mu A/cm^2$ and that of three CS specimens was 1.52 $\mu A/cm^2$. In addition, Figure 7 also shows that the E_{oc} values[2] of SS with oxide scales were noticeably higher (by ~100 mV) than those of SS rebar with sandblasted surface.

[2] It is noted that because of the current averaging processing used, the actual E_{oc} values differed somewhat from those apparent in Figure 7. However, the relative positions of the actual E_{oc} values for the different cases remained the same.

The effect of temperature and pH on cathodic behavior apparently was secondary compared to that of the presence of oxide scales formed at high temperatures (i.e. 700°C). When the temperature of SPS1 was increased from room temperature to 40±2°C, as shown in Figure 8.a, the E_{oc} of sandblasted SS rebar decreased slightly (e.g. ~30 mV) and the CPP curve shifted slightly to the right. This observation is similar to that reported by Jaggi et al.[9] When the pH of testing solution was increased from 12.6 (SPS1) to 13.5 (SPS2), as shown in Figure 8.b, only a small change in the CPP curves was observed and the E_{oc} of sandblasted SS rebar decreased ~ 40 mV.

When the chloride concentration of SPS1 s increased from 0% to up to 3 wt.%, as shown in Figure 9, the CPP curves of the sandblasted SS rebar shifted to the right indicating an increase in oxygen reduction rate. Some of that increase was lost upon further increase of chloride concentration to 5 and 8 wt.% but the oxygen reduction rates in those cases were still higher than in the chloride-free solution. The values of E_{oc} remained largely unchanged, and EIS measurements indicated that the specimens were passive all the time despite the increase of chloride concentration. The initial marked net increase in oxygen reduction rates is against the known trend of decreasing solubility of oxygen in water with increasing NaCl concentration,[13-14] so further investigation of this behavior is needed. Reduced solubility may nevertheless be responsible for the observed beginning of a reversal at the highest chloride concentrations.

When the immersion time in SPS1 increased, the E_{oc} of all the twelve sandblasted SS specimens increased indicating enhanced passivity, [15] which was confirmed by the EIS measurements showing increasing values of Rp (Table 3). Interestingly, as shown in Figure 10, the CPP curves of sandblasted SS rebar shifted somewhat to the left (lower cathodic reaction rate at a given potential) with immersion time. Jaggi et al [9] observed a similar effect of immersion time on SS specimens with ground surfaces.

However, as also shown in Figure 10, the CPP curves of as-received SS rebar instead shifted to the right with increasing immersion time indicating enhance cathodic current at a given potential. A similar effect of immersion time on the cathodic behavior of SS rebar with oxide scales formed at 700 or 1000°C was also observed.

Figure 11 compares typical CPP curves of as-received CS and sandblasted CS in SPS 1. The as-received condition showed higher cathodic efficiency with some increase as immersion time increased (as seen in the SS with oxide scale), and somewhat steeper apparent Tafel slope (~190 mV/dec compared with ~ 130 mV/dec for the sandblasted condition).

Figure 12 shows typical EIS spectra of sandblasted SS and as-received CS rebar in SPS1.

DISCUSSION

Cathodic Efficiency Criterion

Cathodic current density measured at -400 mV (i_{-400}) was used as a criterion to assess the relative cathodic efficiency of SS and CS. That potential was chosen as it is in the order of the

potential adopted by actively corroding rebar in many field conditions. Given that most CPP curves had similar Tafel slopes as those in Figure 1, the relative ranking per i_{-400} would apply also at nearby potentials in the range commonly encountered by corroding rebar.

Estimation of Electrochemical Parameters

In general, the main cathodic reaction taking place on the surface of steel (SS or CS) in concrete and simulated concrete pore solutions is expected to be oxygen reduction with the following half-cell reaction [16]

$$O_2 + 2H_2O + 4e^- = 4OH^- \quad (2)$$

The equilibrium potential E^o of this reaction can be estimated from the Nernst equation,[17]

$$E^o = E^s + \frac{RT}{4F}\ln\frac{P_{o_2}}{[OH^-]^4} \quad (3)$$

where E^s is the equilibrium potential of this reaction at standard conditions, F is the Faraday constant, and Po_2 is the partial pressure of oxygen in atm. In a typical atmospheric environment where Po_2= 0.21 atm, this equation can be simplified to

$$E^o \sim 0.985 - 0.059 \cdot pH \ \text{(V vs SCE)} \quad (4)$$

The reaction rate i_c of the oxygen reduction reaction can be described using Butler-Volmer kinetics,[18] expressed here using concentrations rather than activities

$$i_c = i_o \cdot \frac{C_s}{C_o} \cdot 10^{\frac{(E-E^o)}{b_c}} \quad (5)$$

where i_o is the exchange current density, with a value consistent with the choice of C_o. For convenience, C_o is defined here as the concentration of O_2 at the bulk of the solution, which is assumed to be in equilibrium with an atmosphere with P_{o2} = 0.21 atm. C_s is the concentration of O_2 in the solution immediately next to the rebar surface. When oxygen reduction is under activation control, $C_o \sim C_s$. E is the potential, and b_c is the cathodic Tafel constant.

E^o values were calculated from Equation 4 and values of b_c were estimated from CPP curves as described earlier. Values of i_o were estimated by extrapolation of the Tafel regions of CPP curves.

Table 4 lists estimated values of E^o as well as i_o and b_c of different rebars in SPS1. Because b_c was found to be approximately the same for most of the tested rebars, the magnitude of i_o can be then used as an indicator of cathodic efficiency measuring the effect of composition, high temperature oxide scales, immersion time and chloride concentration on cathodic behavior. The corresponding responses likely reflect variations in surface microstructure as well as electronic properties of the surface films. [19] The mechanistic issues associated with those changes are outside the scope of the present paper and are the subject of separate investigations [19].

Cathodic Efficiency of SS

Figure 13 summarizes all the i_{-400} data for SS and CS rebar in SPS1 (2 day immersion) at –400mV. The cathodic efficiency of these materials can be accordingly divided into three groups in a decreasing order:

1. SS with oxide scales formed 700°C, as-received CS and sandblasted CS rebar
2. SS with oxide scales formed at 1000°C and as-received SS
3. Sandblasted SS

Because the cathodic efficiency of as-received SS was found to be much smaller than that of black bar, it can be concluded that the galvanic coupling between a corroding CS and a pickled condition passive SS rebar could be less troublesome than the coupling between active and passive CS rebars. This observation is in agreement with previous research documented in the literature [4,5,9,20].

However, the cathodic efficiency of the SS rebar was found to depend strongly on its surface condition. When the SS rebar had oxide scales formed at 700°C (simulating the effect of welding), its cathodic efficiency became comparable or even higher than that of as-received CS rebar. This observation is in agreement with Bertolini et al. [4-5] The 1000°C scale had no such drastic effect but the duplicate tests performed showed somewhat greater i_{400} than the as-received condition. Whereas the 1000°C condition represented generally a hot rolling scenario, variability in actual mill conditions and heating schedules in the last rolling steps could easily result in surface properties representative of the 700°C case as well. Therefore, from the point of view of cathodic effects, the high temperature oxide scales formed on the surface of SS rebar may be conservatively assumed to be detrimental. It is cautioned that the above trends on surface condition of SS are inferred from exploratory tests, so larger scale evaluations should be conducted in continuation studies. Further work should also assess the extent to which those effects could be minimized during production, and to determine which subsequent surface cleaning procedures would be required to optimize performance of the final product.

CONCLUSIONS

1. Most cathodic polarization curves of the tested specimens were found to have an apparent Tafel slope of ~ 130 mV/dec. Carbon steel in the as-received "Black bar" condition, however, had an apparent Tafel slope of 190 mV/dec. The mild polarization regime of interest did not cause significant concentration polarization.

2. The cathodic efficiency in simulated concrete pore solution of sandblasted or as-received SS rebar was found to be much smaller than that of as-received CS rebar. Thus the galvanic coupling between passive SS rebar with sandblasted or as-received surface and active CS thus is expected to be less detrimental than the coupling between active and passive CS.

3. Exploratory tests indicated that high temperature oxide scales, especially those formed at 700 °C, significantly increased the cathodic efficiency of SS. The effect of

temperature and pH on cathodic efficiency of sandblasted SS rebar was secondary compared to that of the presence of oxide scales formed at high temperatures.

4. The cathodic efficiency decreased slightly with time for sandblasted SS rebar, but increased significantly with time for SS and CS with high temperature oxide scales or as-received surfaces.

5. Chloride ions increased the cathodic rate on sandblasted SS up to 3 wt.% but less so at higher concentrations.

ACKNOWLEDGEMENT

The authors would like to acknowledge University of South Florida for providing financial support to this study.

REFERENCES

1. G. G. Clemeña and Y.P. Virmani, “Comparing the Chloride Resistances of Reinforcing Bars,” Concrete International, November, 2004: p. 39-49
2. R.N. Cox, J.W. Oldfield, “The Long-Term Performance of Austenitic Stainless Steel in Chloride Contaminated Concrete,” Proc. 4th Int. Symp. on Corrosion of Reinforcement in Concrete Construction, eds. C.L. Page, P.B. Bamforth, J.W. Figg (Cambridge, U.K.:Society of Chemical Industry, 1996): p. 662.
3. P. Castro-Borges et al., "Performance of a 60-Year-Old Concrete Pier with Stainless Steel Reinforcement", Materials Performance, October, 2002: p.50-55
4. L. Bertolini, P. Pedeferri, T. Pastore, “Stainless Steel in Reinforced Concrete Structures”, Proceedings of the 2nd International Conference on Concrete under Severe Conditions, 1998, Eds, Gjørv, O.E., Sakai, K. and Banthia, N. (London, UK: E&FN Spon): p.94-103
5. L. Bertolini, M. Gastaldi, M. Pedeferri, P. Pedeferri, and T. Pastore, “Effects of Galvanic Coupling between Carbon Steel and Stainless Steel Reinforcement in Concrete” Proceedings of International Conference on Corrosion and Rehabilitation of Reinforced Concrete Structures, 1998, Federal Highway Administration Publication No. FHWA-SA-99-014, (Mclean, Virginia: FHWA)
6. L. Bertolini, M. Gastaldi, T. Pastore, and M. Pedeferri, “Corrosion Behavior of Stainless Steel in Chloride Contaminated and Carbonated Concrete” International Journal for Restoration of Buildings and Monuments, 3, 2000: p.273-292
7. P. Pedeferri, L. Bertolini, F. Bolzoni, T. Pastore “Behavior of Stainless Steels in Concrete”, Proceedings of the International Seminar Workshop and Exhibition—Repair and Rehabilitation of Reinforced Concrete Structures: The State of the Art 1997, Eds, Silva-Araya, W.F., De RincóN, O.T. and O’Neill, L.P., (Reston, Virginia: ASCE): p. 192-206
8. P. Pedeferri, “Behavior of Stainless Steel in the Rehabilitation of Corrosion Damaged Infrastructures and Effects of Galvanic Coupling Between Carbon Steel and Stainless Steel” Rehabilitation of Corrosion Damaged Infrastructure, Chapter I: Case and Laboratory Studies, 1998, (Houston, Texas: NACE): p.1-7

9. S. Jaggi, B. Elsener and H. Böhni, “Oxygen Reduction on Mild Steel and Stainless Steel in Alkaline Solutions”, Corrosion of Reinforcement in Concrete, European Federation of Corrosion Publications, Number 31, EUROCORR’99, 1999: p.1-12
10. M. Stern, A.L. Geary, J. Electrochem. Soc. 104, 1 (1957): p. 56.
11. C. Andrade, V. Castelo, C. Alonso, J.A. Gonzalez, “The Determination of the Corrosion Rate of Steel Embedded in Concrete by the Polarization Resistance and AC Impedance Methods,” Conf. Corrosion Effect of Stray Currents and the Techniques for Evaluating Corrosion of Rebars in Concrete (West Conshohocken, PA: ASTM International, 1984), p. 43.
12. A.N. Moosavi, G. John, G. Gedge, “Assessment of Corrosion of Refrigerant Tubes in a Reinforced Concrete Ice Rink Using Corrosion Mapping,” Conf. Corrosion and Corrosion Protection of Steel in Concrete, vol. 1 (Sheffi eld, U.K.: Sheffield Academic Press,1994), p. 116.
13. Cramer, S.D. (1983). “Oxygen Solubility in Brines”, Industrial & Engineering Chemistry Process Design and Development, 23(3): p. 618-620
14. Franchini, M., Unvala, H., Carstensen, J.T. (1993). “Effect of Electrolytes on Oxygen Solubility in Aqueous Systems”, Journal of Pharmaceutical Sciences, 82(5): p. 550
15. F. Cui, Corrosion Behavior of Stainless Steel Clad Rebar, University of South Florida PhD Dissertation 2003
16. A.A. Sagüés, “Critical Issues in Electrochemical Corrosion Measurement Techniques for Steel in Concrete” CORROSION/1991, Paper No. 141, (Houston, Texas: NACE International)
17. D.A. Jones, Principles and Prevention of Corrosion, Prentice-Hall Inc., Upper Saddle River, NJ (1996)
18. D.D. Macdonald, Transient Techniques in Electrochemistry, Plunum Press, New York (1981)
19. A.A. Sagüés, S. Virtanen, P. Schmuki, “Oxygen Reduction on Passive Steel and Cr-Rich Alloys for Concrete Reinforcement,” in Passivation of Metals and Semiconductors, and Properties of Thin Oxide Layers, eds. P. Marcus, V. Maurice (Burlington, MA: Elsevier, Inc., 2006): p. 305.
20. C.M. Abreu, M.J. Cristóbal, M.F. Montemor, X.R. Nóvoa, G. Pena, and M.C. Pérez, Electrochimica Acta, 47 (2002): p. 2271-2279

Table 1
Chemical Composition (%) of Rebars

	C	Si	Cr	Ni	Mn	N	Cu	Mo	Fe
Type 316LN SS	0.01	0.34	16.34	10.24	1.71	0.12	0.61	2.11	Bal.
CS	0.37	0.23	0.19	<0.005	1.24	--	0.34	0.02	Bal.

Table 2
Chemical Composition (g/l) and pH Values of Model Solutions

	$Ca(OH)_2$*	NaOH	KOH**	pH
SPS1	2.0	-	-	12.6
SPS2	2.0	8.33	20.16	13.5

*Most of the $Ca(OH)_2$ was not dissolved
**Reagent grade KOH had only a purity of 85.3%

Table 3
Values of Equivalent Circuit Components Estimated from EIS
(Specimens immersed in SPS1, surface ~ 90 cm^2)

Materials	Time (days)	E_{oc} (V)	Frequency (Hz)*	Rs**	Y_o ($\Omega^{-1}s^n$)	n	R_p (Ω)	i_{corr} ($\mu A/cm^2$)
Sandblasted SS	2	-0.256	0.003	5.2	0.0047	0.906	46745	0.012
Sandblasted SS	259	-0.108	0.00053	4.1	0.0149	0.937	86894	0.007
As received CS	3	-0.147	0.001	7.2	0.0071	0.710	9530	0.061

* The lowest frequency used to fit the experimental data (last five low frequency points used in analysis)
** Estimated from modulus at ~100Hz

Table 4
Electrochemical Parameters Estimated from Tests in SPS1

	Sandblasted Surface		As-received surface		*SS @ 1000C*	*SS @ 700C*
	SS	CS	SS	Black bar		
E^o (V)	0.24	0.24	0.24	0.24	0.24	0.24
i_o (A/cm^2)	$3.4\cdot10^{-12}$	$1.5\cdot10^{-11}$	$5.8\cdot10^{-13}$	$6.4\cdot10^{-10}$	$4.5\cdot10^{-12}$	$3.0\cdot10^{-11}$
b_c (mV/dec)	~130	~130	~110	~190	~130	~130

* As-received Type I CS rebar; ** average value of all the replicates

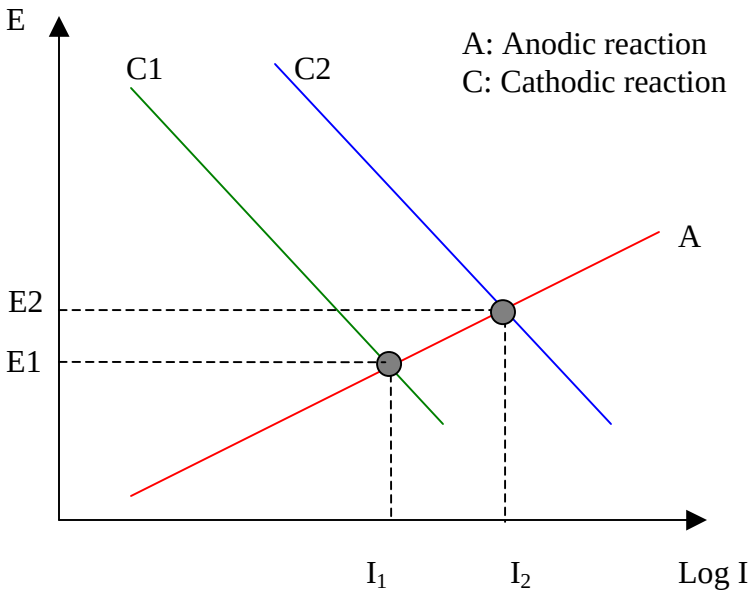

Figure 1. Idealized galvanic coupling scenarios

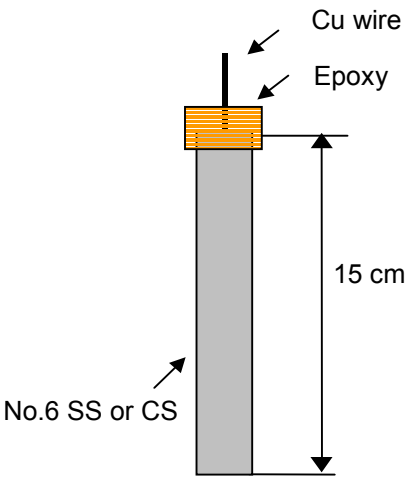

Figure 2. Rebar Specimen Configuration

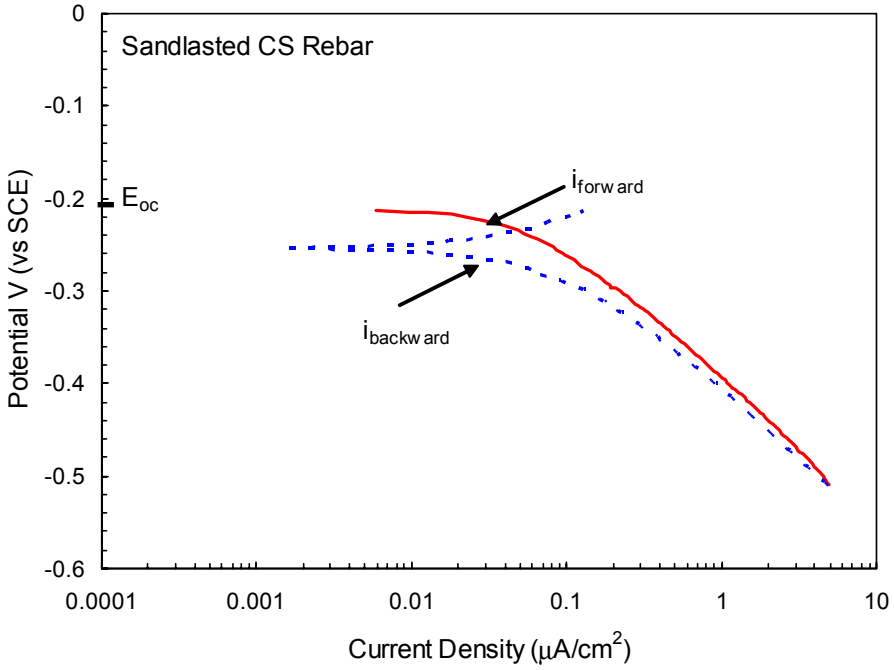

Figure 3. Typical Cyclic Potentiodynamic Polarization (CPP) Curve (Sandblasted CS Rebar in SPS1, 0.167mV/s scan rate)

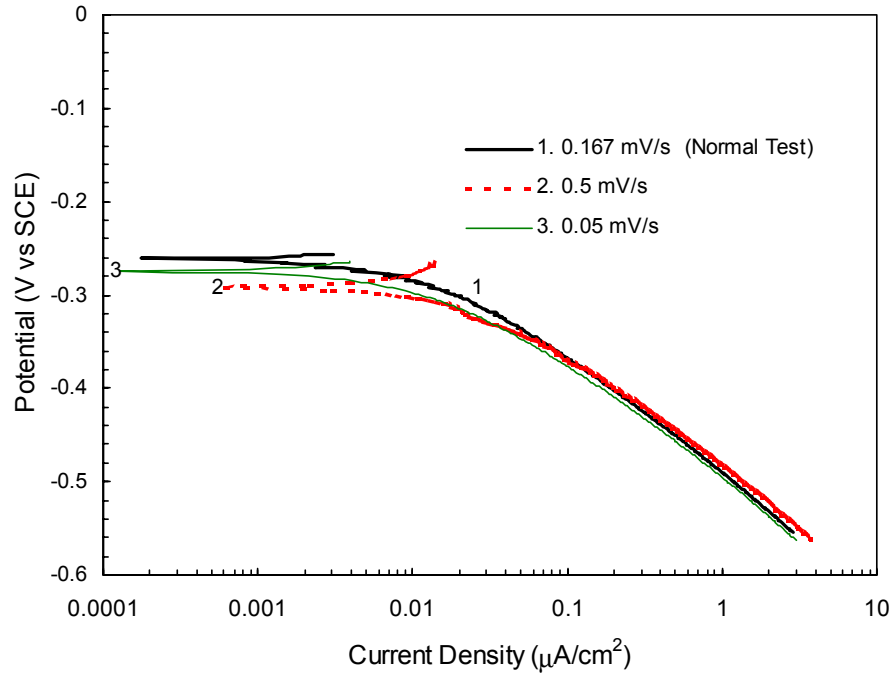

Figure 4. Scan Rate Effect on CPP Curves of Sandblasted SS Rebar in SPS1

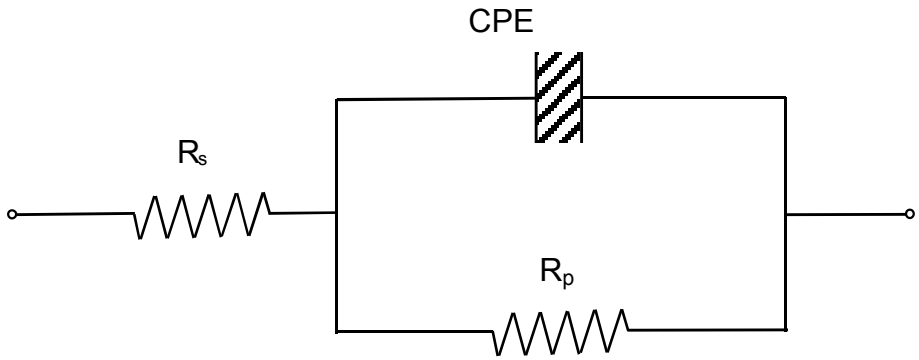

R_s: solution resistance
R_p: polarization resistance
CPE: constant phase angle element ($Z=Y_o^{-1}(j\omega)^{-n}$)

Figure 5. Equivalent Circuit Used to Interpret the EIS Results

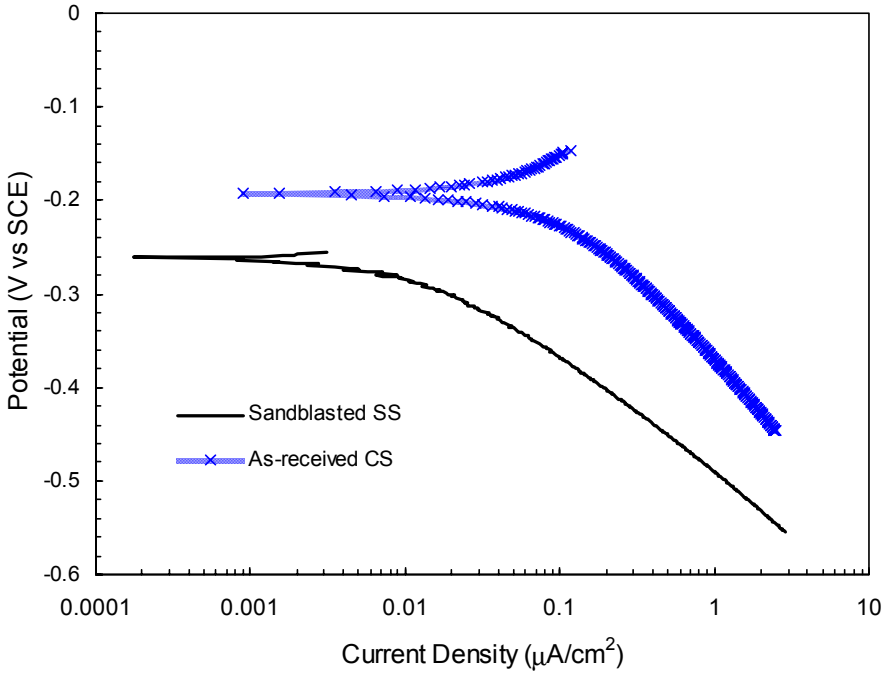

Figure 6. Cathodic Behavior of Sandblasted SS Rebar in SPS1 Comparing with As-Received CS Rebar (Typical Results)

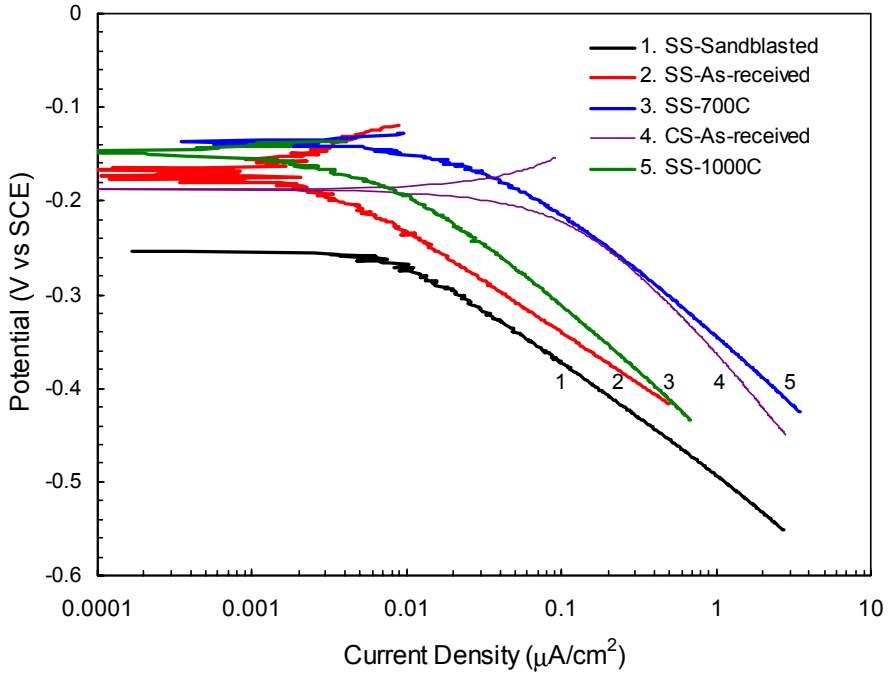

Figure 7. Cathodic Behavior of SS with Various Surface Conditions in SPS1 Comparing with As-received CS Rebar (Typical Results)

(a) (b)

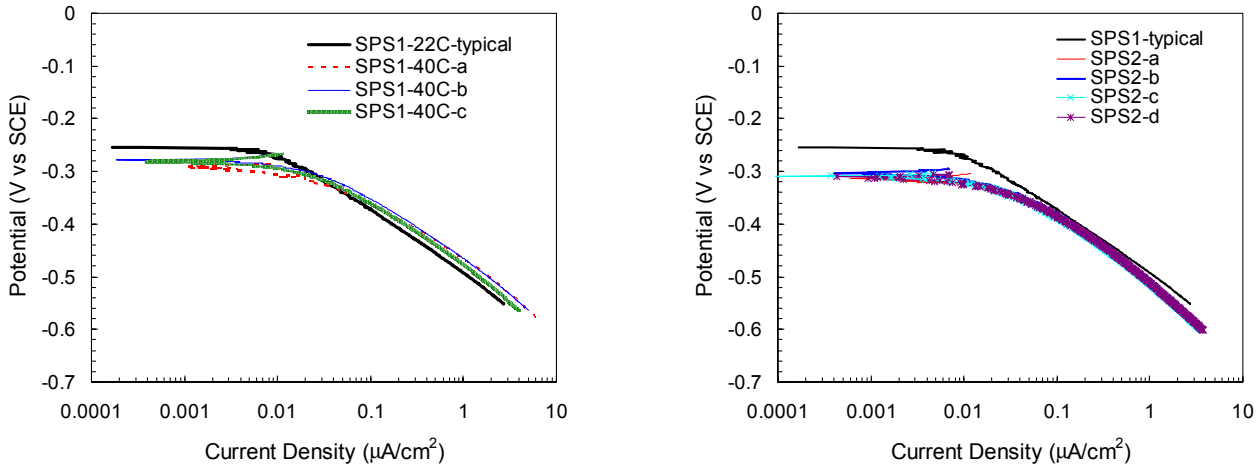

Figure 8. Temperature and pH Effect on Cathodic Behavior of Sandblasted SS Rebar

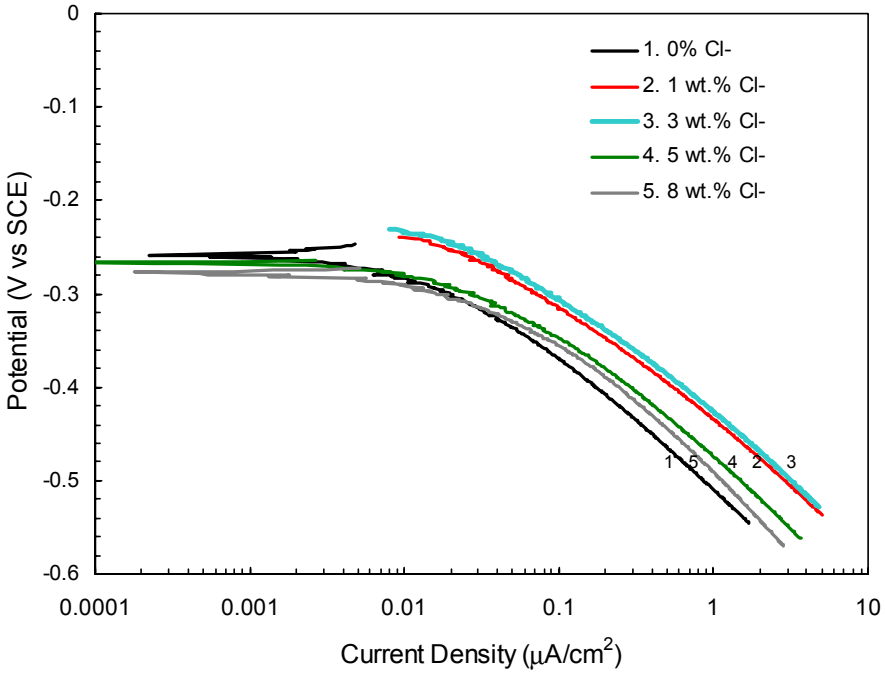

	Current Density ($\mu A/cm^2$)	
0 wt.% Cl^-	0.17	0.19
1 wt.% Cl^-	0.55	0.46
3 wt.% Cl^-	0.64	0.60
5 wt.% Cl^-	0.29	0.27
8 wt.% Cl^-	0.24	0.23

Figure 9. Chloride Effect on Cathodic Behavior of Sandblasted SS Rebars in SPS1

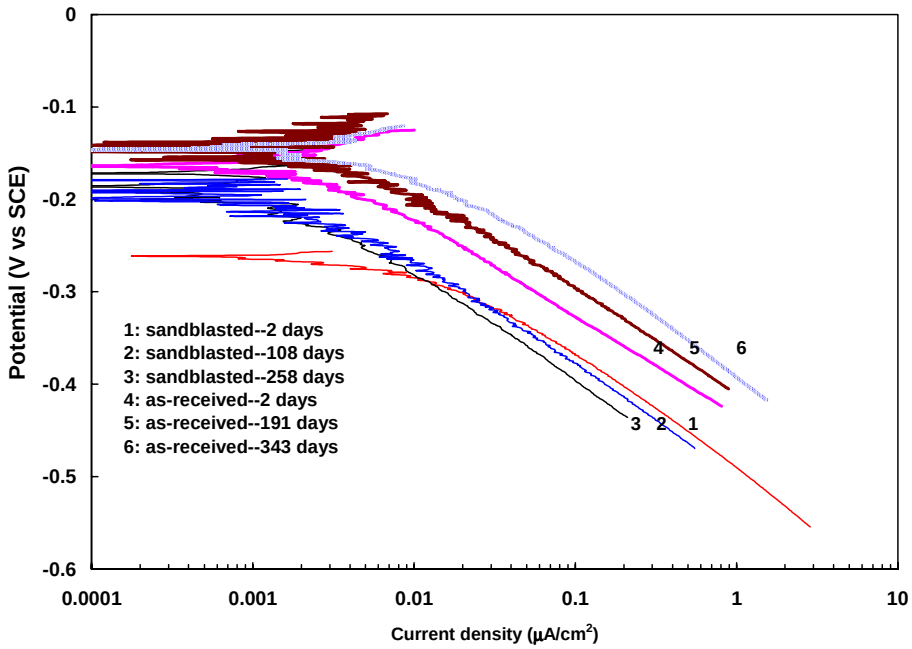

	Current Density ($\mu A/cm^2$)		
SB-2d	0.19	0.19	
SB-108d	0.19	0.19	
SB-258d	0.10	0.10	
AS-2d	0.48	0.35	0.35
AS-94d	0.76	0.76	0.81
AS-343d	1.13	0.80	0.86*

*Extrapolated

Figure 10 Time Effect on Cathodic Behavior of SS Rebars in SPS1 (SB: sandblasted; AS: as-received)

	Current Density ($\mu A/cm^2$)[1]		
As-received-2d	0.82	0.62	0.84
As-received-150d	1.27	0.99	1.14

[1] current densities at -0.35V vs SCE

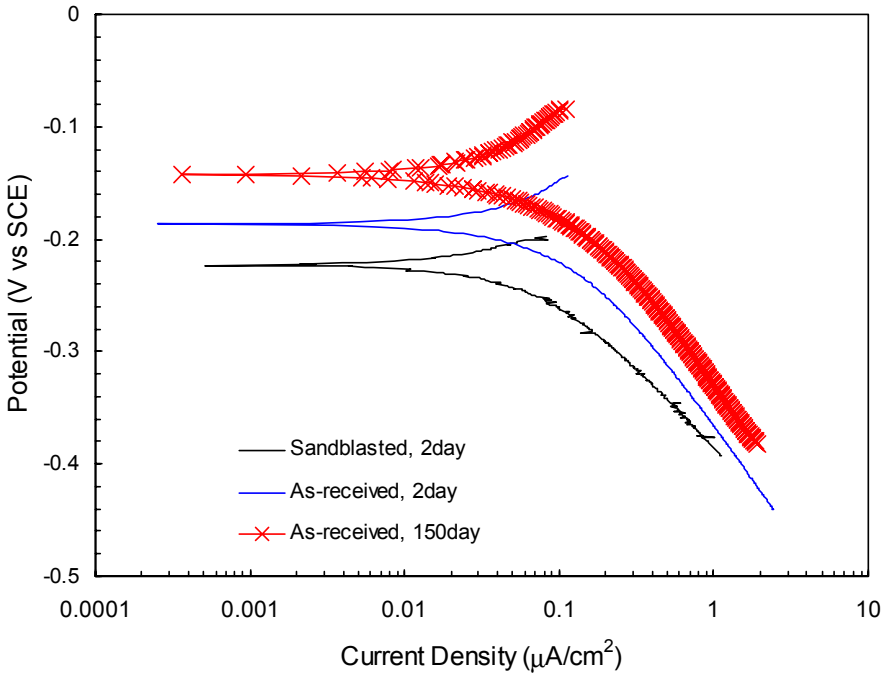

Figure 11. Cathodic Behavior of CS Rebar in SPS1

(a)

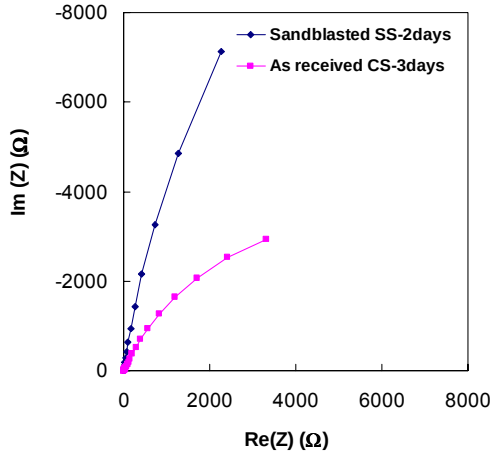

(b)

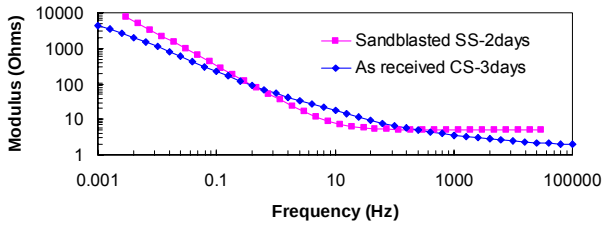

(c)

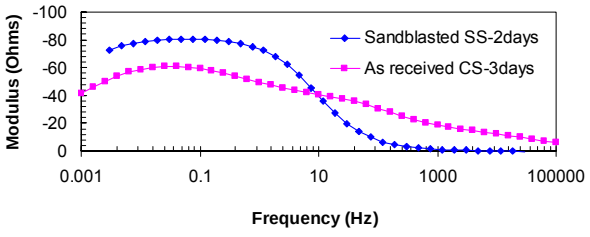

Figure 12. Typical EIS of Rebars in SCS (Surface area ~90 cm^2)

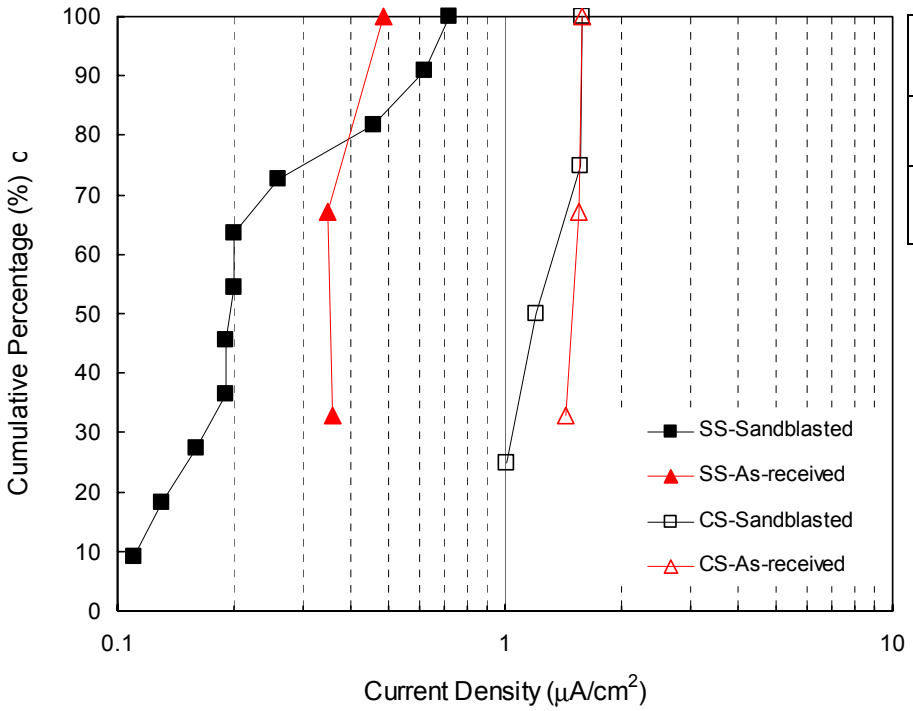

	Current Density (μA/cm^2)	
SS @ 700^{o}C	2.78	2.4
SS @ 1000^{o}C	0.41	0.36

Figure 13. Cathodic Current Density of Different Rebars in SPS1 at –400 mV